Journal of Power Sources 242 (2013) 202–207

Contents lists available at SciVerse ScienceDirect

Journal of Power Sources

journal homepage: www.elsevier.com/locate/jpowsour

Short communication

Study of local disorder in LiMn(Cr,Ni)O_2 compounds by extended X-ray absorption fine structure measurements

L. Maugeri [a], A. Iadecola [a,b], L. Simonelli [c], G. Chen [d], H. Wadati [e], T. Mizokawa [f,g], N.L. Saini [a,*]

[a] Dipartimento di Fisica, Università di Roma "La Sapienza", P. le Aldo Moro 2, 00185 Roma, Italy
[b] Elettra, Sincrotrone Trieste, Strada Statale 14, Km 163.5, Basovizza, Trieste, Italy
[c] European Synchrotron Radiation Facility, 6 RUE Jules Horowitz BP 220, 38043 Grenoble Cedex 9, France
[d] Department of Materials Science, College of Materials Science and Engineering, Jilin University, Changchun 130012, People's Republic of China
[e] Department of Applied Physics and Quantum-Phase Electronics Center (QPEC), University of Tokyo, Hongo, Tokyo 113-8656, Japan
[f] Department of Physics, University of Tokyo, 5-1-5 Kashiwanoha, Kashiwa, Chiba 277-8561, Japan
[g] Department of Complexity Science and Engineering, University of Tokyo, 5-1-5 Kashiwanoha, Kashiwa, Chiba 277-8561, Japan

HIGHLIGHTS

- Local disorder in LiMn(Cr,Ni)O_2 and effect of Mn-site substitution.
- The Jahn-Teller distortion in LiMn(Cr,Ni)O_2 is suppressed by Cr and Ni substitutions
- The near neighbor distances get stiffer with the Cr and Ni substitutions.
- The nature of static configurational disorder is different in the Cr and Ni substituted compounds.

ARTICLE INFO

Article history:
Received 12 January 2013
Received in revised form
10 May 2013
Accepted 11 May 2013
Available online 20 May 2013

Keywords:
Lithium-ion batteries
Local disorder
X-ray absorption spectroscopy
Disordered solids

ABSTRACT

We have studied local structure of $LiMnO_2$, $LiMn_{0.65}Cr_{0.35}O_2$ and $LiMn_{0.5}Ni_{0.5}O_2$ compounds by Mn K-edge extended X-ray absorption fine structure measurements. The local structure of $LiMnO_2$ is found to be consistent with Jahn–Teller distorted MnO_6 octahedra characterized by two different Mn–O bond distances. The Jahn–Teller distortions are suppressed in the Cr and Ni substituted compounds, resulting a single Mn–O distance. However, the Cr atoms tend to occupy a site at a longer distance from Mn in the host lattice (Mn–Cr distance is longer than Mn–Mn distance), unlike the Ni atoms which prefer a site closer to the Mn atoms (Mn–Ni distance is shorter than Mn–Mn distance). Incidentally, Mn–O and Mn–Mn bonds are substantially stiffer in the Cr and Ni substituted compounds. In addition, the static atomic disorder is confined around Cr atoms in the $LiMn_{0.65}Cr_{0.35}O_2$, that is different from the case of $LiMn_{0.5}Ni_{0.5}O_2$ in which larger static disorder appears in the proximity of the Mn atoms. The results suggest that the differences in the local structure of different compounds should be the likely reason for their differing battery characteristics.

1. Introduction

One of the main tasks in the field of rechargeable Li ion batteries is to enhance charge/discharge rates and to replace highly used Li_xCoO_2 [1–5] cathode material by a suitable and less expensive compound. Isostructural $LiMnO_2$ can be a highly suitable replacement due to higher energy density, lower cost and lower toxicity with respect to the $LiCoO_2$, however, the structure instability is a main limiting factor for its battery characteristics [6,7]. Indeed, $LiMnO_2$ compound goes through a phase transition from orthorhombic to spinel structure during the electrochemical cycle. This is due to the fact that $LiMnO_2$ is characterized by Jahn–Teller distortion, i.e., Mn ion in this system is in the Mn^{3+} state. Indeed, it appears that a part of the Mn^{3+} is getting transformed in the Mn^{4+} state during the charging (delithiation) process, and hence the charge/discharge process is controlled by the Jahn–Teller deformation of the MnO_6 octahedra. This transformation has a direct implication on the reversibility of Li ions diffusion since a part of the Li ions is getting trapped in the lattice distortions [1–5].

* Corresponding author. Tel.: +39 0649914387; fax: +39 064957697.
E-mail addresses: Naurang.Saini@roma1.infn.it, naurang.saini@uniroma1.it (N.L. Saini).

0378-7753/$ – see front matter © 2013 Elsevier B.V. All rights reserved.
http://dx.doi.org/10.1016/j.jpowsour.2013.05.038

The Jahn–Teller distortion in $LiMnO_2$ can be suppressed if Mn is partially substituted by other transition metal ions [7–14]. However, the nature of substitutional disorder, that prevents the $LiMnO_2$ to go through the structural transformation, remains unclear. Here, we have addressed this problem and studied local structure of pristine and partially substituted $LiMnO_2$ materials by extended X-ray absorption fine structure (EXAFS) measurements performed as a function of temperature. EXAFS is an atomic site-specific experimental probe [15], that does not require any long range crystal symmetry, and hence permits to have a direct access to the local atomic structure of wide variety of materials, including the Li-based transition metal oxides [9,13,14,16–25] that are commonly used as cathode materials. In this work, we have used Mn K-edge EXAFS to explore local structure of $LiMnO_2$ along with Cr substituted ($LiMn_{0.65}Cr_{0.35}O_2$) and Ni substituted ($LiMn_{0.5}Ni_{0.5}O_2$) compounds. The EXAFS measurements have been performed as a function of temperature to distinctly identify the static configurational disorder from the thermal disorder.

2. Experimental details

Polycrystalline samples of $LiMnO_2$, $LiMn_{0.65}Cr_{0.35}O_2$ and $LiMn_{0.5}Ni_{0.5}O_2$ compounds were synthesized by the solid state reaction method. The details of synthesis and characterization of the samples are reported elsewhere, including the battery characteristics as well as the phase purity and average structure parameters obtained by X-ray diffraction [26,27]. Temperature dependent Mn K-edge X-ray absorption measurements were performed in the transmission mode at the beamline BM23 of the European Synchrotron Radiation Facility (ESRF), Grenoble. The synchrotron radiation emitted by a bending magnet source at 6 GeV ESRF storage ring was monochromatized by a double crystal Si(311) monochromator. The samples were mounted in a continuous flow He cryostat and the temperature was controlled and monitored within an accuracy of ±1 K. Several scans were acquired at each temperature to ensure the spectral reproducibility. Standard procedure based on spline fit of the pre-edge subtracted absorption spectrum was used to extract the EXAFS signal [15].

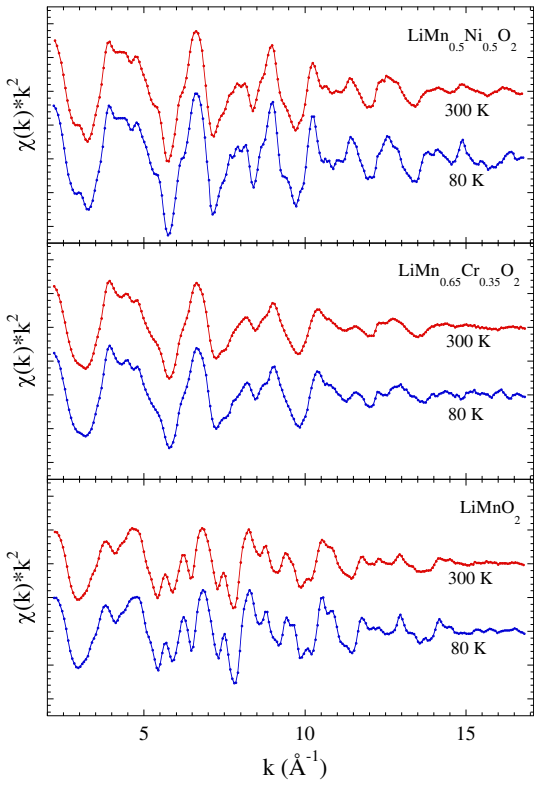

Fig. 1. Mn K-edge EXAFS oscillations (weighted by k^2) measured on $LiMnO_2$ (lower), $LiMn_{0.65}Cr_{0.35}O_2$ (middle) and $LiMn_{0.5}Ni_{0.5}O_2$ (upper) compounds at two temperatures (80 K and 300 K).

3. Results and discussion

Fig. 1 shows EXAFS oscillations at two different temperatures (80 K and 300 K), extracted from Mn K-edge X-ray absorption spectra measured on pristine $LiMnO_2$ and the Cr ($LiMn_{0.65}Cr_{0.35}O_2$) and Ni ($LiMn_{0.5}Ni_{0.5}O_2$) substituted compounds. The EXAFS oscillations are multiplied by k^2 to enhance the amplitude in the higher k-region. The oscillations can be seen clearly even at high temperature and there are some apparent differences in the EXAFS

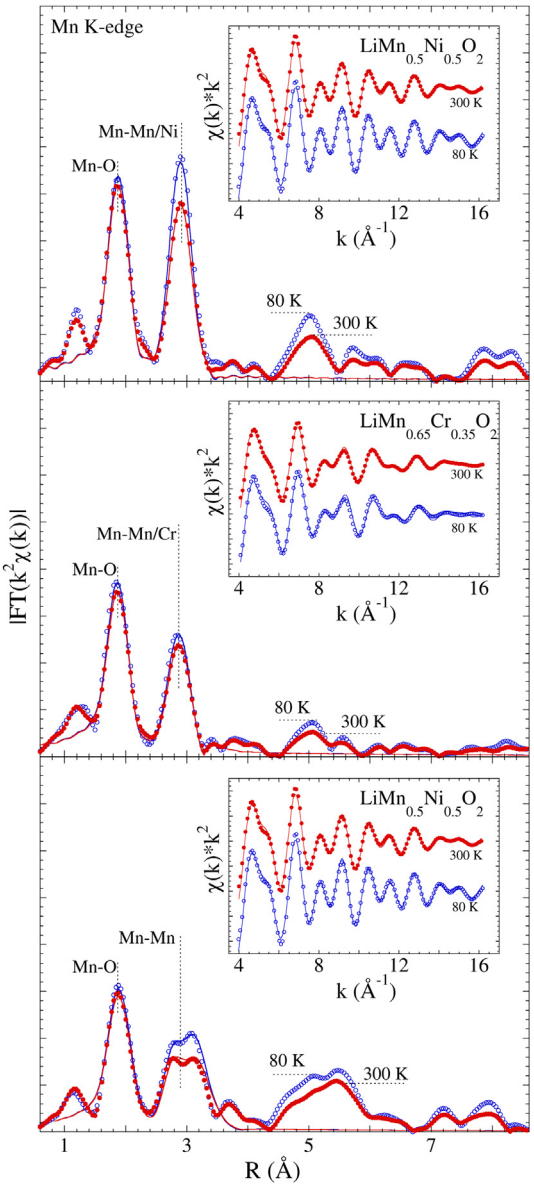

Fig. 2. Fourier transform magnitudes of the k^2-weighted Mn K-edge EXAFS of $LiMnO_2$ (lower), $LiMn_{0.65}Cr_{0.35}O_2$ (middle) and $LiMn_{0.5}Ni_{0.5}O_2$ (upper) compounds at two temperatures (80 K and 300 K). The insets show the filtered EXAFS oscillations with the model fits using Mn–O and Mn–Mn/Cr/Ni shells. Model fits in the real space (solid curves) is also included.

oscillations of three compounds. The differences can be further appreciated in the Fourier transform (FT) of EXAFS oscillations, providing real-space information.

Fig. 2 shows the FT magnitudes of the EXAFS oscillations. The FTs are performed in the k range of 3–16 Å^{-1} using a Gaussian window. The FTs provide information on the atomic distribution around the photoabsorbing Mn atoms in the LiMn(Cr,Ni)O_2 compounds. The contributions of nearest neighbour O atoms (at a distance ~1.9 Å), and next nearest neighbour Mn/Ni/Cr atoms (at a distance ~2.9 Å) appear as two main FT peaks. The FT peaks at longer distances are due to multiple scattering contributions. Apparently there is hardly any change in the peak positions with temperature, however, the amplitude appears suppressed at higher temperature due to higher thermal disorder. The peaks due to Mn–O and Mn–Mn in the pristine $LiMnO_2$ are largely damped due to Jahn–Teller distortion in this compound. Indeed, the Mn–Mn peak has a doublet structure in the $LiMnO_2$ due to two distinct Mn–Mn distances in this compound. There is a clear change in the Mn–O peak amplitude with the partial substitution of Mn by Cr and Ni, higher for the substituted samples due to the fact that Jahn–Teller distortion in these samples is suppressed. It can be seen that the Ni substituted compound has smaller disorder, evident from higher EXAFS and FT amplitude in compare to the other two compounds.

To determine local structure parameters a theoretical modelling of the EXAFS oscillations is necessary. In the single-scattering approximation, the EXAFS oscillations can described by the following general equation [15]:

$$\chi(k) = \sum_i \frac{N_i S_0^2}{kR_i^2} f_i(k,R_i) e^{-\frac{2R_i}{\lambda}} e^{-2k^2\sigma_i^2} \sin[2kR_i + \delta_i(k)] \quad (1)$$

where N_i is the number of neighbouring atoms at a distance R_i, δ_i is the phase shift, $f_i(k,R_i)$ is the backscattering amplitude, λ is the photoelectron mean free path, and σ_i^2 is the correlated Debye–Waller factor (DWF) measuring the mean square relative displacements (MSRDs) of the photoabsorber-backscatter pairs. The S_0^2 is the so-called passive electrons reduction factor, i.e., EXAFS amplitude reduction factor due to many-body effects related with the losses occurring during the photoelectron propagation in the material (excitations as plasmons, electron–hole pairs, etc.) and the intrinsic losses due to shake-up and shake-off excitations created by the core–hole in the absorption process. While it is difficult to quantify these many-body effects, chemical transferability is best procedure for the estimation of S_0^2 [15,28].

In the Mn K-edge EXAFS of LiMn(Cr,Ni)O2 compounds, contributions of Mn–O and Mn–Mn/Ni/Cr bondlengths are well separated from any multiple scattering (Fig. 2) and hence we can analyse them separately. We have used EXCURVE 9.275 code (with calculated backscattering amplitudes and phase shift functions) for the EXAFS model fits [29]. Only the radial distances R_i and the corresponding σ_i^2, were allowed to vary in the least squares fits using a model of two shells (i.e., Mn–O and Mn–Mn/Cr/Mn distances). The Ni were fixed to the known values from average structure measured by diffraction [27,30,31]. The E_0 and S_0^2 were fixed after a number of fit trials on four different scans at 300 K on the pristine $LiMnO_2$ compound. The best fit values for the S_0^2 were found to be 0.8 for Mn–O shell and 1.0 for Mn–Mn and Mn–Cr/Ni shells. These values are consistent with the available EXAFS literature on oxides revealing S_0^2 to be between 0.7 and 0.9 for metal–oxygen and 0.8–1.0 for the metal–metal pairs [28,32,33]. The number of independent data points, $N_{ind} \sim (2\Delta k \Delta R)/\pi$ [15] were about 18 ($\Delta k = 12$ Å^{-1} and $\Delta R = 2.4$ Å), for the maximum of eight parameters fits. The uncertainties were determined by creating correlation maps with appropriate contour level established by

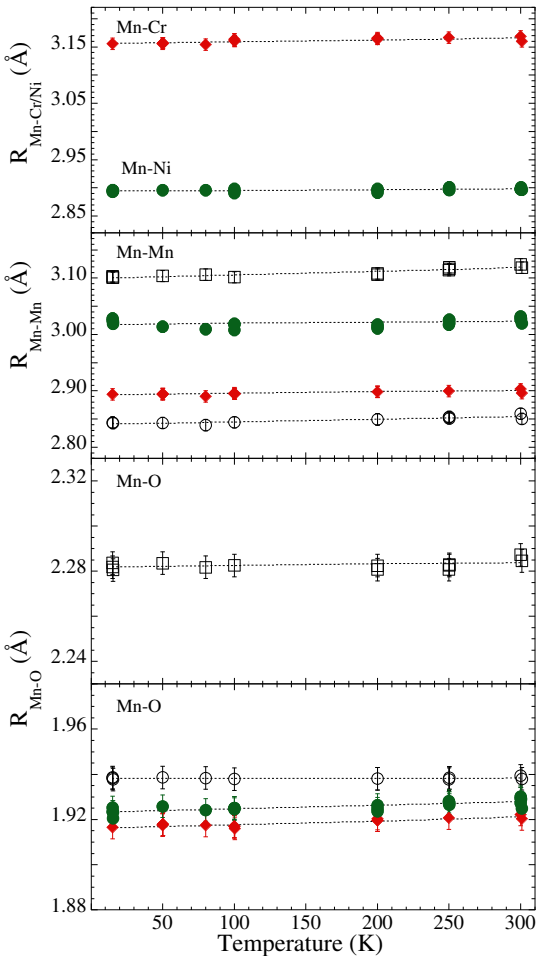

Fig. 3. Mn–O and Mn–Mn/Cr/Ni distances determined by Mn K-edge EXAFS analysis as a function of temperature. The data from $LiMnO_2$ are shown by empty symbols (black), while the red filled diamonds ($LiMn_{0.65}Cr_{0.35}O_2$) and green filled circles ($LiMn_{0.5}Ni_{0.5}O_2$) represent the substituted samples. The distance scale interval for the upper two panels (Mn–Mn/Cr/Ni distances) is four times the interval in the lower two panels (Mn–O distances). Duplicate symbols at some temperatures correspond to the data obtained at different time interval using a different setup. (For interpretation of the references to colour in this figure legend, the reader is referred to the web version of this article.)

modelling four different scans at a constant temperature. The contribution of Mn–Li distance (~2.97 Å) is ignored due to negligible X-ray scattering factor of lithium in compare to Mn and other transition metals (Cr, Ni). The model fits in the real space using two shells are shown in Fig. 2. The k-space model fits of Fourier filtered EXAFS are also included in Fig. 2 as an inset.

Fig. 3 shows temperature dependence of different bondlengths determined by the EXAFS analysis. The resulting bondlengths indicate that the local structure of $LiMnO_2$ is characterized by two distinct Mn–O distances (four atoms at ~1.94 Å, and two atoms at ~2.29 Å) and two different Mn–Mn distances (~2.86 Å, and ~3.12 Å) consistent with Jahn–Teller distortion (see e.g., empty symbols in Fig. 2). The bondlengths are slightly different from diffraction studies [30,31] that show three Mn–O distances (two atoms each at ~1.90 Å, ~1.95 Å, and ~2.30 Å) and two Mn–Mn distances (~2.81 Å, and ~3.10 Å), however, consistent with other local structure studies [13]. Unlike the $LiMnO_2$, the Cr and Ni substituted compounds show only a single Mn–O distance due to suppression of Jahn–Teller distortion (see, e.g. filled diamonds and filled circles respectively in Fig. 2). The Mn–O bondlengths in the substituted compounds are slightly contracted with respect to the

Table 1
Local structure parameters of $LiMnO_2$, $LiMn_{0.65}Cr_{0.35}O_2$ and $LiMn_{0.5}Ni_{0.5}O_2$ compounds determined by Mn K-edge EXAFS. The values of near neighbour distances are provided for 300 K. Maximum uncertainty in distance determination is ∼0.01 Å, and for the σ_0^2 is ∼0.0005 Å^2.

		$LiMnO_2$		$LiMn_{0.65}Cr_{0.35}O_2$	$LiMn_{0.5}Ni_{0.5}O_2$
Mn–O	R (Å)	1.94	2.29	1.92	1.93
	θ_E (K)	587(48)	455(20)	705(98)	701(72)
	σ_0^2 (Å^2)	0.0004	0.0022	0.0006	0.0000
Mn–Mn	R (Å)	2.86	3.11	2.90	3.02
	θ_E (K)	345(24)	326(20)	468(102)	494(104)
	σ_0^2 (Å^2)	0.0018	0.0043	0.0046	0.0161
Mn–Cr/Ni	R (Å)	–	–	3.16	2.90
	θ_E (K)	–	–	424(60)	416(42)
	σ_0^2 (Å^2)	–	–	0.0068	0.0002

short Mn–O bonds in the pristine $LiMnO_2$, consistent with an increase of average valence of Mn in the substituted compounds.

The Mn–Mn bondlength in the Cr substituted, $LiMn_{0.65}Cr_{0.35}O_2$, compound (∼2.90 Å) is nearly equal (slightly longer) to the shorter Mn–Mn bondlength (∼2.86 Å) in the Jahn–Teller distorted $LiMnO_2$ compound. This is different from the case of Ni substituted, $LiMn_{0.5}Ni_{0.5}O_2$ compound, in which the Mn–Mn bondlength (∼3.02 Å) appears slightly shorter than the longer Mn–Mn bondlength (∼3.12 Å) in $LiMnO_2$ compound. On the other hand, Mn–Cr distance (∼3.16 Å) is much longer than the Mn–Mn distance (∼2.90 Å) in $LiMn_{0.65}Cr_{0.35}O_2$. Again, this is different from $LiMn_{0.5}Ni_{0.5}O_2$ compound in which the Mn–Mn and Mn–Ni distances are found to be ∼3.02 Å, and ∼2.90 Å, respectively. The near neighbour distances measured by Mn K-edge EXAFS at 300 K in three compounds are summarized in Table 1. The Mn–Cr and Mn–Ni distances were also determined by Cr K-edge and Ni K-edge EXAFS (not shown here), found to be consistent with those measured by Mn K-edge EXAFS. Within the experimental uncertainties, the near neighbour distances hardly show any change with temperature (Fig. 3).

Further information on the atomic disorder can be obtained by the distance broadening measured by the EXAFS Debye–Waller factors (σ^2), i.e. the MSRDs of the near neighbour distances. Fig. 4 shows temperature dependence of the σ^2 determined by modelling of EXAFS oscillations due to Mn–O and Mn–Mn/Cr/Ni distances. The σ^2 is sum of temperature independent (σ_0^2) and temperature dependent ($\sigma^2(T)$) terms, i.e. $\sigma^2 = \sigma_0^2 + \sigma^2(T)$. While σ_0^2 describes the static configurational disorder, the temperature dependent $\sigma^2(T)$ is generally given by the correlated Einstein (or Debye) model [15]. However, in the harmonic and single scattering approximation the simplest model to describe the $\sigma^2(T)$ is the correlated Einstein model, and the difference with the Debye model is smaller than experimental and theoretical uncertainties in the low temperature regime [34,35]. The Einstein equation to describe the $\sigma^2(T)$ is given as:

$$\sigma^2(T) = \frac{\hbar^2}{2\mu k_B \theta_E} \coth \frac{\theta_E}{2T} \quad (2)$$

The Einstein temperatures (θ_E, i.e., the Einstein frequency $\omega_E k_B \theta_E/\hbar$) for the Mn–O distance are higher for the substituted samples, indicating larger force constants for the Mn–O bondlengths in these compounds (the effective force constant k is given by $k = \mu\omega_E^2$, where μ is the reduced mass and ω_E the Einstein frequency of the pair of atoms). Indeed, the Einstein temperatures for the Mn–O bondlengths in $LiMnO_2$ are found to be 587 ± 48 K and 455 ± 20 K respectively for the shorter and longer bonds. However, the θ_E for the Mn–O pairs in $LiMn_{0.65}Cr_{0.35}O_2$ and $LiMn_{0.5}Ni_{0.5}O_2$ are much larger, ∼705 ± 98 K and ∼701 ± 72 K respectively. Therefore, the Mn–O bondlengths are stiffer in the substituted compounds, likely to be due to suppressed Jahn–Teller distortions. The estimated force constants are ∼16.7 eV Å^{-2} and ∼10 eV Å^{-2} respectively for the shorter and longer Mn–O bondlengths of the $LiMnO_2$, and substantially higher ∼24 eV Å^{-2} for the sole Mn–O bondlengths in the Cr and Ni substituted compounds.

Also, the θ_E for Mn–Mn bondlengths in the substituted samples are substantially different from that in the pristine $LiMnO_2$. Indeed, θ_E for the Mn–Mn bondlengths in the $LiMnO_2$ (345 ± 24 K and 326 ± 20 K) are found to be much smaller than the one for the Cr and Ni substituted compounds (468 ± 102 K and 494 ± 104 K respectively). In the $LiMnO_2$, the two Mn–Mn bondlengths have almost similar force constants ∼5.2 eV Å^{-2}, however, different static disorder (σ_0^2 ∼0.002 Å^2 and 0.004 Å^2 respectively for the short and long Mn–Mn bonds). It is interesting to note that the θ_E of Mn–Mn bondlengths in the Cr substituted sample is much larger, however, the static disorder is essentially similar (σ_0^2 ∼0.005 Å^2) to the longer Mn–Mn bonds in the pristine $LiMnO_2$. The situation is

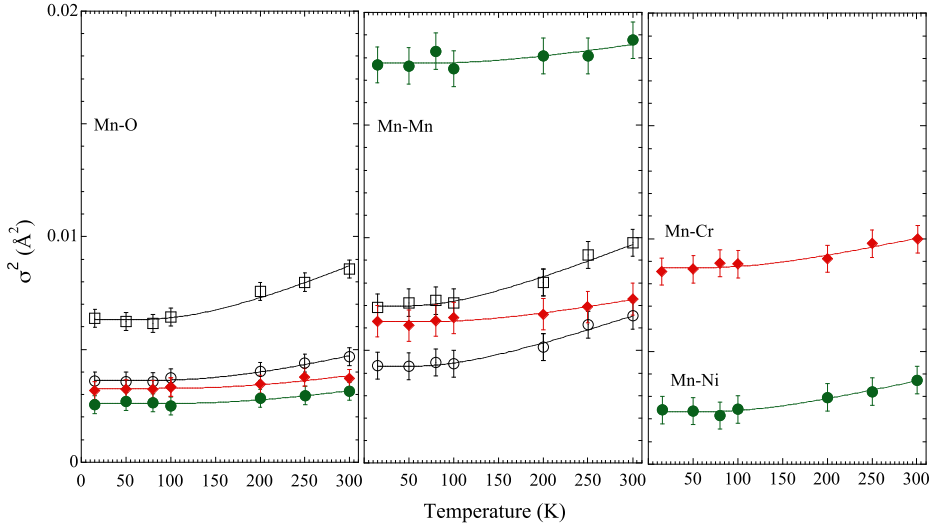

Fig. 4. Temperature dependence of Mn–O (left), Mn–Mn (middle) and Mn–Cr/Ni (right) MSRDs for $LiMnO_2$ (black open symbols), $LiMn_{0.65}Cr_{0.35}O_2$ (green filled circles) and $LiMn_{0.5}Ni_{0.5}O_2$ (red filled diamonds). The solid curves represent the correlated Einstein model fits to the data. (For interpretation of the references to colour in this figure legend, the reader is referred to the web version of this article.)

very different for the Ni substituted compound in which the static disorder for the Mn–Mn bonds is much larger (σ_0^2 ~0.016 Å^2), consistent with large configurational disorder around the Mn site in the $LiMn_{0.5}Ni_{0.5}O_2$, albeit the θ_E for the Mn–Mn remains similar to the one in the Cr substituted compound.

Unlike the Mn–Mn, the Mn–Ni bondlengths hardly suffer any static disorder (σ_0^2 ~0.0002 Å^2) with the θ_E (~416 ± 42 K) for this Mn–Ni bond being very similar to the Mn–Mn bondlength in the $LiMnO_2$. On the other hand, Mn–Cr bondlength has larger static disorder (σ_0^2 ~0.007 Å^2), with the θ_E (~424 ± 60 K) being slightly larger than the one for the Mn–Ni bond in Ni substituted system. Therefore, there is a larger static disorder around the substituted Cr site (Mn–Cr bonds) in the $LiMn_{0.65}Cr_{0.35}O_2$ unlike the Ni substituted system in which the large static disorder is confined around the Mn site (Mn–Mn bonds) and not around the substituted Ni site (Mn–Ni bonds). The Cr K-edge EXAFS (measuring Cr–Mn and Cr–Cr correlations) and Ni K-edge EXAFS (measuring Ni–Mn and Ni–Ni correlations) data further support the results obtained by the Mn K-edge EXAFS data discussed here. The σ_0^2 and the Einstein-temperatures for different bondlengths are also summarized in Table 1.

Let us discuss possible implications of the present results. The EXAFS data reveal that the force constants of the Mn–O and Mn–Mn bondlengths are substantially increased with partial substitution of Mn in $LiMnO_2$, consistent with suppression of Jahn–Teller distortion in this compound. The suppression of Jahn–Teller distortion implies that the Mn is in the Mn^{4+} ($3d^3$) state in the substituted ($LiMn_{0.65}Cr_{0.35}O_2$ and $LiMn_{0.5}Ni_{0.5}O_2$) compounds and, as expected, a contraction of Mn–O bondlength is observed. Although, both Cr and Ni substitutions suppress the Jahn–Teller distortion, the nature of atomic disorder due to these substitutions is very different. For example, the static disorder in the $LiMn_{0.65}Cr_{0.35}O_2$ seems confined around the Cr sites while that in the $LiMn_{0.5}Ni_{0.5}O_2$ is likely to be around the Mn and not around the Ni site. Here, it is worth recalling that the Cr and Ni are the redox centres in the substituted compounds [24]. Therefore, it is likely that the Mn^{4+} with confined static disorder around it remaining inert while the Ni^{2+} acting as redox centre in the $LiMn_{0.5}Ni_{0.5}O_2$ (system behaving as if $LiNiO_2$). On the other hand, there is a larger disorder around the substituted Cr in the $LiMn_{0.65}Cr_{0.35}O_2$ system, and being the redox centre the large disorder around Cr^{3+} in $LiMn_{0.65}Cr_{0.35}O_2$ has substantial effect on the battery characteristics. This may be the reason why the $LiMn_{0.5}Ni_{0.5}O_2$ system is preferable as cathode for lithium ion batteries unlike the $LiMn_{0.65}Cr_{0.35}O_2$. Furthermore, soft X-ray absorption measurements [26] have revealed that Cr in $LiMn_{0.65}Cr_{0.35}O_2$ is in Cr^{3+} state while Ni in $LiMn_{0.65}Cr_{0.35}O_2$ is in Ni^{2+} state. It was concluded that Cr creates Li deficiency in the $LiMn_{0.65}Cr_{0.35}O_2$. In the light of present results it appears that Li deficiency due to Cr^{3+} is giving rise to a larger static disorder confined around the Cr in $LiMn_{0.65}Cr_{0.35}O_2$ and hence a limiting factor for the use of Cr substituted system as cathode material.

In summary, we have studied local structure of $LiMnO_2$, $LiMn_{0.65}Cr_{0.35}O_2$ and $LiMn_{0.5}Ni_{0.5}O_2$ compounds by temperature dependent Mn K-edge EXAFS measurements. We have observed Jahn–Teller distortion, shown by two Mn–O and two Mn–Mn bond distances in the $LiMnO_2$ system, and suppression of the Jahn–Teller distortion by partial substitution at the Mn site, resulting a single Mn–O distance. We find that the substitution of Cr introduces a larger static disorder around the Cr site unlike the Ni substituted system in which a larger static disorder is confined around the Mn site. The local Mn–O and Mn–Mn bonds get stiffer in the substituted systems. The results suggest that static disorder around the Cr and Mn sites in the $LiMn_{0.65}Cr_{0.35}O_2$ and $LiMn_{0.5}Ni_{0.5}O_2$ should be key to limit the efficiency of Li ion batteries. Indeed, the presence of Cr ions prevents the possibility of a reversible diffusion process for Li^+ ions, which appear to get trapped around the Cr ions (and hence large static disorder). In contrast, the presence of Ni^{2+} provides greater Li^+ ion mobility and hence $LiMn_{0.5}Ni_{0.5}O_2$ can have better diffusion properties than the Cr substituted system and the Jahn–Teller distorted $LiMnO_2$ compound.

Here, we should mention that the Mn^{3+} formation in $LiNi_{0.5}Mn_{1.5}O_4$ spinel promotes Ni–Mn site disorder, that is shown to facilitate the Li^+ transport, especially in the high rate regimes [36]. Indeed, a comparison of the electrochemical performances with different Mn^{3+} contents demonstrates that a careful control of the amount of the Jahn-Teller Mn^{3+} ions and, thus, the disordered phase, is the key for high performance spinel cathode materials. Comparing with the present findings on the local structure, we have found that the static disorder in the Ni substituted $LiMnO_2$ is around the Mn site unlike the case of Cr substituted system in which the Mn site contains smaller disorder as the disorder is confined around the Cr site. Therefore, co-substitution, i.e., a partial Cr substitution in $LiMn_{0.5}Ni_{0.5}O_2$ can be used to control and improve stability of the cathode materials. This is consistent with the detailed experimental and theoretical study by Xiao et al. [36], suggesting that $LiNi_{0.45}Cr_{0.05}Mn_{1.5}O_4$ is more stable than $LiNi_{0.5}Mn_{1.5}O_4$. Nevertheless, the present report makes a further point on the important role of local site disorder due to partial substitution of Ni and Cr in the $LiMnO_2$ cathode materials.

Acknowledgements

The authors wishes to thank ESRF staff for the help and support during the experimental runs. This research is partially supported by the Japan Society for the Promotion of Science (JSPS) through the 'FIRST Program' initiated by the Council for Science and Technology Policy.

References

[1] M. Yoshio, R.J. Brodd, A. Kozawa (Eds.), Lithium Ion Batteries – Science and Technologies, Springer, 2009.
[2] J.-M. Tarascon, M. Armand, Nature 414 (2001) 359. and references therein.
[3] J.B. Goodenough, Y. Kim, Chem. Mater. 22 (2010) 587.
[4] Bruno Scrosati, Jurgen Garche, J. Power Sources 195 (2010) 2419.
[5] P. He, H. Yu, D. Li, H. Zhou, J. Mater. Chem. 22 (2012) 3680.
[6] Y.-J. Gu, Y.-B. Chen, H.-K. Wu, Y.-M. Wang, L. Chen, M. Wang, X.-W. Huang, H. Zheng, X.-B. Liu, Ch. Lu, Y. Hu, Energy Mater. 4 (2009) 40.
[7] A. Manthiram, J. Choi, W. Choi, Solid State Ionics 177 (2006) 2629.
[8] G. Ceder, S.K. Mishra, Electrochem. Solid-State Lett. 2 (1999) 550.
[9] R. Prasad, R. Benedek, M.M. Thackeray, Phys. Rev. B 71 (2005) 134111. R. Prasad, R. Benedek, A.J. Kropf, C.S. Johnson, A.D. Robertson, P.G. Bruce, M.M. Thackeray, Phys. Rev. B 68 (2003) 012101.
[10] Z.P. Guo, S. Zhong, G.X. Wang, H.K. Liu, S.X. Dou, J. Alloys Compd. 348 (2003) 231.
[11] M. Gateshki, S.-Ju Hwang, D.H. Park, Y. Ren, V. Petkov, J. Phys. Chem. B 108 (2004) 14956.
[12] X.M. Wu, R.X. Li, S. Chen, Z.Q. He, M.F. Xu, Bull. Mater. Sci. 31 (2008) 109.
[13] S.-J. Hwang, H.-S. Park, J.-H. Choy, Solid State Ionics 151 (2002) 275. S.-J. Hwang, H.-S. Park, J.-H. Choy, Chem Mater. 12 (2000) 1818.
[14] M.G. Kim, H.J. Shin, J.-H. Kim, S.-H. Park, Y.-K. Sunb, J. Electrochem. Soc. 152 (2005) A1320.
[15] R. Prins, D.C. Koningsberger (Eds.), X-ray Absorption: Principles, Applications, Techniques of EXAFS, SEXAFS, XANES, Wiley, New York, 1988.
[16] L. Maugeri, A. Iadecola, B. Joseph, L. Simonelli, L. Olivi, M. Okubo, I. Honma, H. Wadati, T. Mizokawa, N.L. Saini, J. Phys. Condens. Matter 24 (2012) 335305.
[17] L. Maugeri, L. Simonelli, A. Iadecola, B. Joseph, M. Okubo, I. Honma, H. Wadati, T. Mizokawa, N.L. Saini, J. Power Sources 229 (2013) 272.
[18] J. McBreen, J. Solid State Electrochem. 13 (2009) 1051.
[19] A.V. Chadwick, S.L.P. Savin, R. Alcantara, D.F. Lisbona, P. Lavela, G.F. Ortiz, J.L. Tirado, ChemPhysChem 7 (2006) 1086.
[20] T. Nedoseykina, S.-S. Kim, Y. Nitta, Electrochim. Acta 52 (2006) 1467.
[21] W.-S. Yoon, K.-K. Lee, K.-B. Kim, J. Electrochem. Soc. 149 (2002) A146.
[22] P. Shearing, Y. Wu, S.J. Harris, N. Brandon, Electrochem. Soc. Interface 43 (2011).
[23] Y.W. Tsai, B.J. Hwang, G. Ceder, H.S. Sheu, D.G. Liu, J.F. Lee, Chem. Mater. 17 (2005) 3191.
[24] M. Balasubramanian, X. Sun, X.D.Q. Yang, J. McBreen, J. Power Sources 92 (2001) 1. M. Balasubramanian, X. Sun, X.DQ. Yang, J. McBreen, J. Electrochem. Soc. 147 (2000) 2903.

[25] I.J. Pickering, J. Graham, N. George, J.T. Lewandowski, A.J. Jacobson, J. Am. Chem. Soc. 115 (1993) 4137.
[26] H. Wadati, D.G. Hawthorn, T.Z. Regier, G. Chen, T. Hitosugi, T. Mizokawa, A. Tanaka, G.A. Sawatzky, Appl. Phys. Lett. 97 (2010) 022106.
[27] Z.-F. Huang, F. Du, C.-Z. Wang, D.-P. Wang, G. Chen, Phys. Rev. B 75 (2007) 054411. F. Du, Z.-F. Huang, C.-Z. Wang, X. Meng, G. Chen, Y. Chen, S.-H. Feng, J. Appl. Phys. 102 (2007) 113906.
[28] G.G. Li, F. Bridges, C.H. Booth, Phys. Rev. B 52 (1995) 6332.
[29] S.J. Gurman, J. Synchrotron Radiat. 2 (1995) 56.
[30] A.R. Armstrong, P.G. Bruce, Nature 381 (1996) 499.
[31] J. Akimoto, Y. Takahashi, Y. Gotoh, K. Kawaguchi, K. Dokko, I. Uchida, Chem. Mater. 15 (2003) 2984.
[32] A. Bianconi, N.L. Saini, Struct. Bonding 114 (2005) 287.
[33] M. Filippi, B. Kundys, S. Agrestini, W. Prellier, H. Oyanagi, N.L. Saini, J. Appl. Phys. 106 (2009) 104116.
[34] E. Sevillano, H. Meuth, J.J. Rehr, Phys. Rev. B 20 (1979) 4908.
[35] See, e.g. a review by J.J. Rehr, R.C. Albers, Rev. Mod. Phys. 72 (2000) 621.
[36] J. Xiao, X. Chen, P.V. Sushko, M.L. Sushko, L. Kovarik, J. Feng, Z. Deng, J. Zheng, G.L. Graff, Z. Nie, D. Choi, J. Liu, J.-G. Zhang, M.S. Whittingham, Adv. Mater. 24 (2012) 2109.